http://dx.doi.org/10.18623/rvd.v23.5894

APPLYING REMOTE SENSING IMAGE INTERPRETATION TO ANALYZE RIVERBANK CHANGES: A CASE STUDY IN THE MEKONG DELTA

APLICAÇÃO DA INTERPRETAÇÃO DE IMAGENS DE SENSORIAMENTO REMOTO PARA ANALISAR ALTERAÇÕES NAS MARGENS DOS RIOS: UM ESTUDO DE CASO NO DELTA DO MEKONG

Article received on: 11/20/2025
Article accepted on: 2/19/2026

Luu Van Ninh*
* Hanoi University of Science VNU, Hanoi, Vietnam
luuninhtv@gmail.com

Nguyen Huu Tuan**
**Ho Chi Minh City University of Natural Resources and Environment, Ho Chi Minh City, Vietnam
nhtuan@hcmunre.edu.vn

Le Thi Kim Thoa**
**Ho Chi Minh City University of Natural Resources and Environment, Ho Chi Minh City, Vietnam
tkkthoa@hcmunre.edu.vn

Doan Quang Tri***
***Institute of Earth Sciences, Vietnam Academy of Science and Technology, Hanoi, Vietnam
Orcid: https://orcid.org/0000-0003-2376-3222
doanquangtrikttv@gmail.com

Vu Cao Dat***
***Institute of Earth Sciences, Vietnam Academy of Science and Technology, Hanoi, Vietnam
datvucao97@gmail.com

Nguyen Ngoc Mong Kha****
******Can Tho University, Can Tho, Vietnam
nnmkha@gmail.com

Bui Xuan Khanh*****
*******Kien Giang University, An Giang, Vietnam
bxkhanh@vnkgu.edu.com

Thu-Van Can**
**Ho Chi Minh City University of Natural Resources and Environment, Ho Chi Minh City, Vietnam
Orcid: https://orcid.org/0009-0007-8114-3853
ctvan@hcmunre.edu.vn

The authors declare that there is no conflict of interest

Abstract
In recent decades, riverbank erosion has intensified in the Mekong Delta, Vietnam, particularly in downstream sections of the Mekong River system, causing significant riverbank morphological changes and threatening infrastructure, ecosystems, and local communities. Monitoring riverbank dynamics is therefore essential for understanding erosion trends and supporting effective management strategies. This study analyzes riverbank changes along eight river segments in An Giang Province

Resumo
Nas últimas décadas, a erosão das margens fluviais intensificou-se no Delta do Mekong, no Vietnã, particularmente nos trechos a jusante do sistema do rio Mekong, causando mudanças morfológicas significativas nas margens e ameaçando a infraestrutura, os ecossistemas e as comunidades locais. O monitoramento da dinâmica das margens fluviais é, portanto, essencial para compreender as tendências de erosão e apoiar estratégias de gestão eficazes. Este estudo analisa as mudanças nas margens

using multi-temporal Landsat and Sentinel-2 satellite imagery at nine time points (1992–2024). Shoreline dynamics were quantified using the Digital Shoreline Analysis System (DSAS) based on the Linear Regression Rate (LRR) and Shoreline Change Envelope (SCE) indices. The results show that erosion dominates most river sections. Erosion accounts for 100% of shoreline change at VT1, VT4, VT7, and VT8; 97.1% at VT2; 99.19% at VT5; and 86.25% at VT6, while limited accretion occurs mainly at VT2, VT3, VT5, and VT6. VT3 records the highest accretion proportion (25.1%), although erosion remains the prevailing trend. SCE results reveal strong spatial variability in shoreline mobility, with the largest changes occurring at VT7 and VT8, where shoreline displacement exceeds 100 m and reaches up to 200 m at VT8. In contrast, VT1, VT2, and VT5 show relatively minor changes (<30 m), indicating greater geomorphological stability. These findings demonstrate the effectiveness of integrating multi-temporal remote sensing data with DSAS for detecting erosion hotspots and supporting riverbank management and early warning systems in the Mekong Delta.

Keywords: Remote Sensing. Riverbank Erosion. Digital Shoreline Analysis System (DSAS). Shoreline Change Detection. Mekong Delta.

ao longo de oito segmentos fluviais na província de An Giang, utilizando imagens de satélite multitemporais do Landsat e do Sentinel-2 em nove momentos (1992–2024). A dinâmica da linha de costa foi quantificada utilizando o Sistema de Análise Digital da Linha de Costa (DSAS), com base nos índices de Taxa de Regressão Linear (LRR) e Envelope de Mudança da Linha de Costa (SCE). Os resultados mostram que a erosão predomina na maioria dos trechos fluviais. A erosão é responsável por 100% da alteração da linha de costa em VT1, VT4, VT7 e VT8. 97,1% em VT2. 99,19% em VT5. e 86,25% em VT6, enquanto a acréscimo ocorre de forma limitada principalmente em VT2, VT3, VT5 e VT6. O VT3 registra a maior proporção de acréscimo (25,1%), embora a erosão continue sendo a tendência predominante. Os resultados do SCE revelam forte variabilidade espacial na mobilidade da linha de costa, com as maiores mudanças ocorrendo nos pontos VT7 e VT8, onde o deslocamento da linha de costa ultrapassa 100 m e chega a 200 m no VT8. Em contrapartida, VT1, VT2 e VT5 apresentam alterações relativamente menores (<30 m), indicando maior estabilidade geomorfológica. Esses resultados demonstram a eficácia da integração de dados de sensoriamento remoto multitemporal com o DSAS para detectar pontos críticos de erosão e apoiar a gestão das margens fluviais e os sistemas de alerta precoce no Delta do Mekong.

Palavras-chave: *Sensoriamento Remoto. Erosão de Margens Fluviais. Sistema de Análise Digital da Linha de Costa (DSAS). Detecção de Alterações na Linha de Costa. Delta do Mekong.*

1 INTRODUTION

Remote sensing has become an essential tool for investigating shoreline dynamics, enabling systematic observation of coastal and riverbank changes over large spatial extents and long temporal scales. The application of satellite-based observations to shoreline change analysis began in the early 1970s with the launch of Earth observation missions such as the Landsat program developed by NASA. Landsat satellites provide medium-resolution multispectral imagery with consistent temporal coverage, creating

one of the longest continuous archives of Earth surface observations available for environmental monitoring. This long-term dataset has enabled researchers to quantify shoreline evolution and identify patterns of erosion and accretion driven by coastal hydrodynamics, sediment transport processes, and human activities. By analyzing multi-temporal Landsat imagery, numerous studies have demonstrated the capability of satellite data to detect and monitor shoreline variability at decadal scales. For example, Morton *et al.* (2005) analyzed historical shoreline changes along the open-ocean coasts of the United States using multi-temporal shoreline datasets and lidar-derived coastlines, revealing significant spatial variability in erosion and accretion rates across the Gulf of Mexico region and highlighting the influence of sediment dynamics and coastal management practices such as beach nourishment.

Remote sensing has become one of the most widely used approaches for monitoring shoreline and riverbank dynamics, particularly through the extraction of shoreline indicators such as the waterline from multi-temporal imagery (Thakur *et al.*, 2017; Abdel Aziz, 2024). By providing consistent observations over large spatial extents and long temporal scales, satellite data enable the assessment of erosion-accretion patterns and the morphodynamic evolution of coastal and fluvial systems. Early studies demonstrated the potential of integrating high-resolution satellite imagery with historical aerial photographs for reconstructing long-term shoreline changes. Chalabi *et al.* (2004) combined IKONOS imagery with aerial photographs from 1966–1994 to analyze shoreline dynamics in Kuala Terengganu, Malaysia, using image segmentation and GIS-based shoreline extraction techniques. Similarly, Marfai *et al.* (2008) integrated historical topographic maps with IKONOS and Landsat imagery to investigate coastal morphodynamics in Semarang, Indonesia, showing that sediment accumulation has dominated shoreline evolution in the region over nearly a century. Landsat imagery has also been widely applied for decadal-scale shoreline monitoring. Tamassoki *et al.* (2014) used Landsat TM-5 data combined with maximum likelihood classification to evaluate shoreline variability in Bandar Abbas, Iran, while Shin and Kim (2015) applied high-resolution satellite images to analyze morphological changes along Gwangan Beach, South Korea.

Remote sensing has also proven effective for investigating riverine processes. Recent advances in geospatial analysis combining multi-temporal satellite imagery and

tools such as DSAS and Google Earth Engine have significantly improved the monitoring and quantification of long-term riverbank erosion and accretion dynamics (Miah *et al.*, 2025). Tan *et al.* (2026) have highlighted that shoreline dynamics in coastal and estuarine systems are highly influenced by variations in sediment supply, hydrodynamic processes, and human interventions, leading to complex patterns of coastal erosion and accretion over time. Jia *et al.* (2026) demonstrated that applying a machine-learning-based super-resolution approach (Real-ESRGAN) to enhance Sentinel-1 SAR imagery can significantly improve the spatial resolution and accuracy of satellite-derived river water level monitoring, enabling reliable large-scale hydrological observations. For example, Hu *et al.* (2021) used time-series Sentinel-1 SAR data and knowledge-based classifiers to produce a 10-m resolution map of coastal salt marshes in China with an overall accuracy of 87%. In addition to satellite observations, emerging technologies such as unmanned aerial vehicles (UAVs) and airborne LiDAR have significantly enhanced the spatial resolution and accuracy of shoreline monitoring. UAV imagery has been used to capture high-resolution coastal morphology and detect short-term shoreline changes (Choi et al., 2016; Novais *et al.*, 2023; Sujivakand *et al.*, 2024). Meanwhile, LiDAR-derived elevation models have enabled detailed analysis of coastal and riverbank topography, supporting the detection of inundation flood, coastal hazard assessments (Liu, 2009; Hladik and Alber, 2012). More recently, geospatial analysis and artificial intelligence techniques have been increasingly integrated with remote sensing to improve shoreline change detection and erosion risk assessment (Karnata and Kumari, 2025). Bordoloi *et al.* (2020) applied geospatial modeling to assess riverbank erosion probability along the Subansiri River in India, while Supattra Puttinaovarat *et al.* (2022) developed a remote sensing and artificial intelligence framework for river classification and change detection using satellite imagery.

Despite significant progress in remote sensing-based shoreline monitoring, several challenges remain, particularly in large and highly dynamic deltaic environments. Most existing studies have focused on coastal shorelines or individual river reaches, while long-term and spatially consistent assessments of riverbank dynamics across complex delta systems remain relatively limited. In the Mekong Delta, rapid riverbank erosion has become an increasingly critical issue due to the combined impacts of hydrological variability, sediment supply reduction, river engineering, and human activities. However,

comprehensive analyses integrating multi-temporal satellite imagery and geospatial techniques to quantify long-term riverbank changes in this region are still insufficient. Therefore, this study aims to apply multi-temporal remote sensing analysis to investigate riverbank line changes in selected areas of the Mekong Delta. The results provide new insights into the spatial patterns and temporal trends of riverbank dynamics, contributing to improved understanding and management of erosion processes in deltaic environments.

In the Mekong Delta, remote sensing has increasingly been applied to investigate shoreline and riverbank dynamics, reflecting the growing concern over erosion processes in this highly dynamic deltaic environment. Studies have reported significant riverbank erosion along the Mekong River branches. For instance, Tha *et al.* (2022) identified severe bank retreat in areas such as Tan Chau and Sa Dec, where erosion rates reached approximately 30 m/year and 42 m/year, respectively. In addition, Binh *et al.* (2020) improved riverbank delineation in the Mekong Delta by integrating Landsat imagery with water indices and a modified automated approach for extracting river and lake boundaries. Similarly, Li *et al.* (2017) utilized a long-term Landsat image archive spanning 43 years (1973–2015) to investigate coastline evolution across the Mekong Delta, demonstrating the effectiveness of multi-temporal satellite observations for detecting large-scale shoreline changes.

In Vietnam, remote sensing and GIS have also been widely applied to monitor shoreline and riverbank variability in different coastal and riverine environments (Tri *et al.*, 2023). Thao *et al.* (2011) applied remote sensing and GIS techniques to monitor and quantify shoreline changes in the Phan Thiết coastal area. Thuy (2012) used similar approaches to analyze erosion and accretion processes along the Hai Phong coastline. At the river basin scale, Long and Khoi (2020) employed remote sensing and GIS to assess riverbank changes in the Mekong and Bassac rivers in the An Giang during the period 1989–2015, highlighting the applicability of multi-temporal satellite imagery for evaluating long-term fluvial dynamics. In addition, Son *et al.* (2015) explored the use of VNREDSat-1 satellite imagery to support the assessment and prediction of geological hazards in large hydropower reservoirs and transportation systems in the mountainous regions of northwestern Vietnam.

Several studies have also focused on shoreline monitoring at river mouths and coastal zones using multi-source satellite imagery. Trung and Khanh (2016) applied multi-temporal Landsat data to monitor shoreline changes in the Cua Dai area of the Thu Bon River, Quang Nam Province. Cuong *et al.* (2018) investigated coastal erosion and accretion processes in the Thừa Thiên Huế coastal zone using remote sensing and GIS techniques. Thi and Thu (2019) used RapidEye imagery (6.5 m spatial resolution) to analyze shoreline erosion at the Da Rang River mouth in Phú Yên during the period 2010–2018. More recently, Tung and Hung (2023) applied Sentinel-2 data to analyze shoreline evolution and seabed topographic changes in the Nhat Le estuary, Quang Binh. Recent studies have also incorporated advanced geospatial analysis tools to improve shoreline change detection. In addition, several other studies in Vietnam have applied remote sensing techniques to investigate the spatial and temporal evolution of riverbanks and coastlines (Tinh and Phong, 2017; Quynh et al., 2018; Long *et al.*, 2019; Thuy *et al.*, 2019; Khoi *et al.*, 2020; Binh *et al.*, 2020; Hau *et al.*, 2022; Phuong *et al.*, 2023). These studies demonstrate the growing application of remote sensing technologies in monitoring geomorphological changes in Vietnam's coastal and riverine systems.

Despite the increasing number of studies applying remote sensing to monitor shoreline and riverbank dynamics, systematic assessments of long-term riverbank changes in highly dynamic deltaic environments remain relatively limited. In the Mekong Delta, riverbank erosion has become an increasingly serious issue due to the combined impacts of hydrological variability, sediment supply reduction, river engineering, and intensive human activities. However, comprehensive analyses that quantify spatial and temporal patterns of riverbank erosion and accretion using multi-temporal satellite observations are still insufficient for many river reaches in this region.

Therefore, this study aims to apply multi-temporal satellite imagery and geospatial analysis techniques to quantify riverbank erosion and accretion rates along several representative river sections in the Mekong Delta. By integrating long-term satellite observations with spatial analysis, this study provides a systematic framework for detecting riverbank changes and offers new insights into the morphodynamic evolution of river systems in highly dynamic deltaic environments.

2 MATERIALS AND METHODS

2.1. Description of study site

The study area is located in An Giang Province, in the upstream region of the Vietnamese Mekong Delta, southern Vietnam. This province lies along the lower reaches of the Mekong River system, where the river divides into two main distributaries in Vietnam: the Tien River and the Hau River. These rivers play a critical role in regional hydrology, sediment transport, and socio-economic development, but they also experience significant riverbank instability due to dynamic fluvial processes. An Giang Province is particularly vulnerable to riverbank erosion because of strong seasonal variations in river discharge, sediment transport dynamics, and increasing anthropogenic pressures such as riverbank engineering and sand mining. In recent years, severe riverbank erosion has occurred in several locations, leading to land loss, infrastructure damage, and threats to local communities.

To investigate long-term riverbank dynamics, eight representative river segments (VT1–VT8) were selected along the Tien and Hau Rivers within An Giang Province. These segments are distributed across areas including Tan Chau, Phu Tan, and Chau Phu, where riverbank erosion has been frequently reported. The selected reaches have lengths ranging from approximately 1.38 km to 1.96 km, representing different geomorphological and hydrodynamic conditions along the river system. The spatial distribution of the study area and the selected monitoring segments is presented in Figure 1, which illustrates the location of the eight riverbank sections (VT1–VT8) analyzed in this study.

Figure 1

Map of the study area

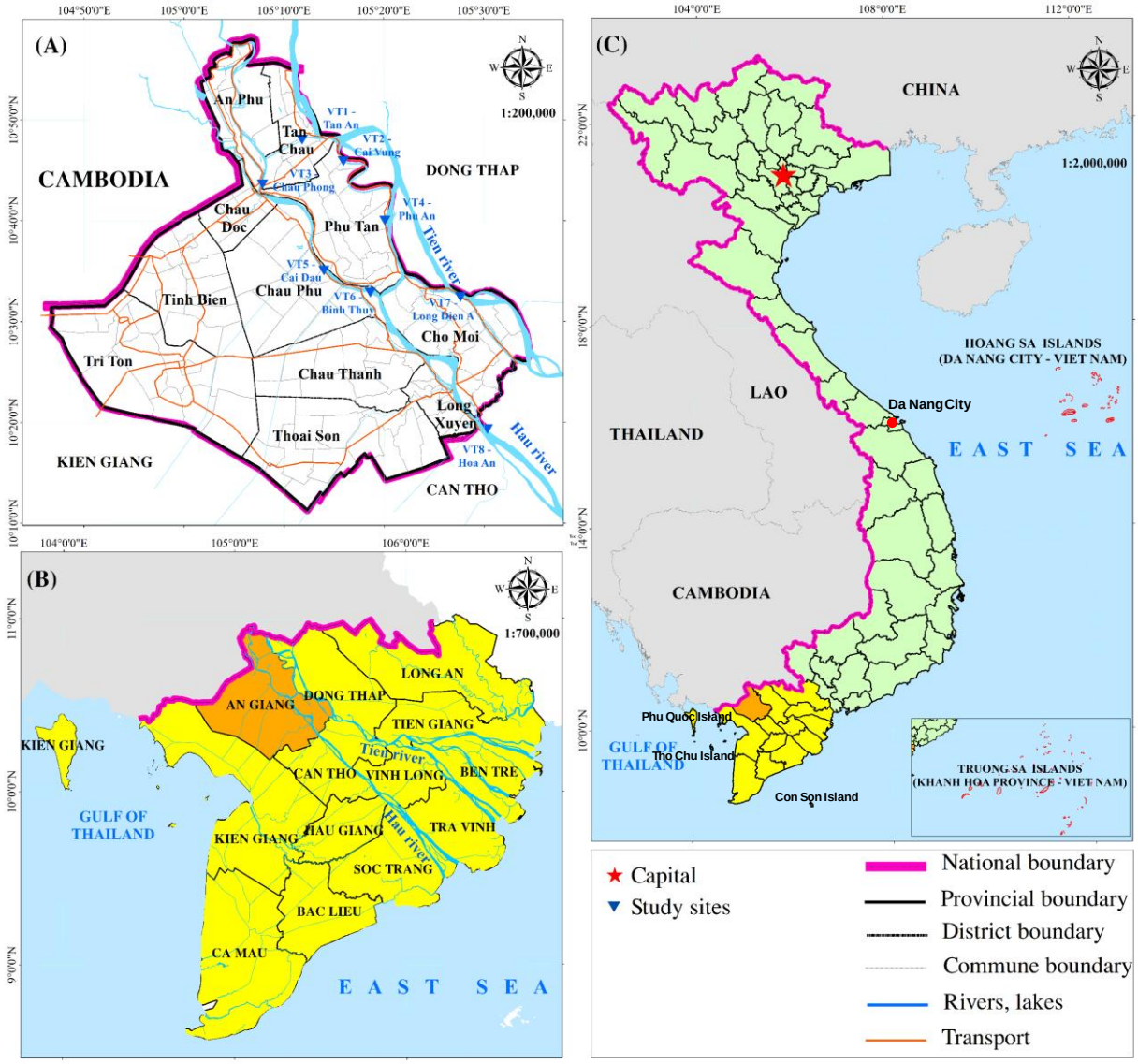

2.2 Methodology

Remote sensing image analysis has been widely applied to monitor shoreline dynamics using various techniques. Among them, water index methods such as the Normalized Difference Water Index (NDWI) and the Modified Normalized Difference Water Index (MNDWI) are commonly used to delineate water bodies and extract shoreline information (McFeeters, 2007; Xu, 2007). By comparing shorelines derived from multi-temporal images, erosion, accretion, and other coastal changes can be

identified through spatial overlay analysis or by calculating variations in water surface extent within a GIS environment. Another widely used approach is the Automated Water Extraction Index (AWEI), which enhances the discrimination of water bodies from other land-cover types, particularly under complex conditions such as moist soils and urban areas, thereby improving the accuracy compared with traditional water indices (Feng et al., 2011). In addition, the Band Ratio (BR) method provides a simple yet effective approach for detecting water bodies and shoreline changes by enhancing spectral contrast between water and other surface features such as soil, vegetation, or built-up areas (Jensen, 1996). More recently, deep learning techniques have emerged as powerful tools for remote sensing analysis, with models such as Convolutional Neural Networks (CNNs) enabling accurate image segmentation and automatic extraction of shoreline-related features.

However, the Digital Shoreline Analysis System (DSAS) has been recognized as an advanced GIS-based tool for quantifying and evaluating shoreline changes over time. DSAS is an extension of ArcGIS developed by the United States Geological Survey, which enables users to calculate shoreline change rates using various statistical approaches. GIS- and remote sensing–based shoreline analysis integrated with the DSAS framework has demonstrated strong effectiveness in investigating coastal dynamics and shoreline variability (Quynh et al., 2022). Numerous studies have applied this approach to assess shoreline evolution in different coastal environments, including Ash Shu'aybah in Saudi Arabia (Alharbi et al., 2023), Monterey Bay in the United States (Bheeroo et al., 2016), and Venice Lagoon in Italy (Al-Zubieri et al., 2020). In addition, DSAS has been successfully used to evaluate shoreline responses to natural hazards, such as along Fire Island (Hapke et al., 2013), the Chandeleur Islands (Mishra et al., 2022), and coastal areas impacted by Hurricane Sandy (Kish and Donoghue, 2013). The DSAS methodology operates by integrating shoreline datasets derived from multiple time periods and applying quantitative statistical techniques to estimate rates of erosion, accretion, and other shoreline dynamics (Thieler et al., 2009; Boak & Turner, 2005; Moore, 2000; USGS, 2021).

a) Shoreline change analysis using the DSAS framework:

Shoreline dynamics were quantified using a GIS-based framework integrating multi-temporal satellite imagery and the Digital Shoreline Analysis System (DSAS)

within the ArcGIS platform. The overall analytical workflow is illustrated in Figure 2, which summarizes the main stages of data processing and shoreline change analysis.

Multi-temporal Landsat and Sentinel-2 Level-2 imagery were used to derive shoreline positions for different observation years. Image preprocessing included radiometric enhancement, geometric correction, and spatial subsetting to the study area to ensure consistent spatial comparability. Shorelines were then extracted using a spectral band-ratio approach designed to enhance the contrast between water and land surfaces. Specifically, shoreline delineation was performed using the ratio between the green and mid-infrared spectral bands (Band 3/Band 7 for Landsat and Band 3/Band 8 for Sentinel-2), which effectively separates water bodies from adjacent land features.

The extracted shoreline datasets were converted into vector format and integrated into the DSAS framework for quantitative analysis. A baseline was established parallel to the general coastline orientation, from which a series of equally spaced transects were generated automatically. These transects were used to measure shoreline displacement through time and to calculate statistical indicators of shoreline change, including the End Point Rate (EPR), Linear Regression Rate (LRR), Weighted Linear Regression (WLR), and Net Shoreline Movement (NSM). Together, these metrics provide a robust assessment of erosion, accretion, and long-term shoreline variability along the study coast.

Figure 2

Methodological framework of the study.

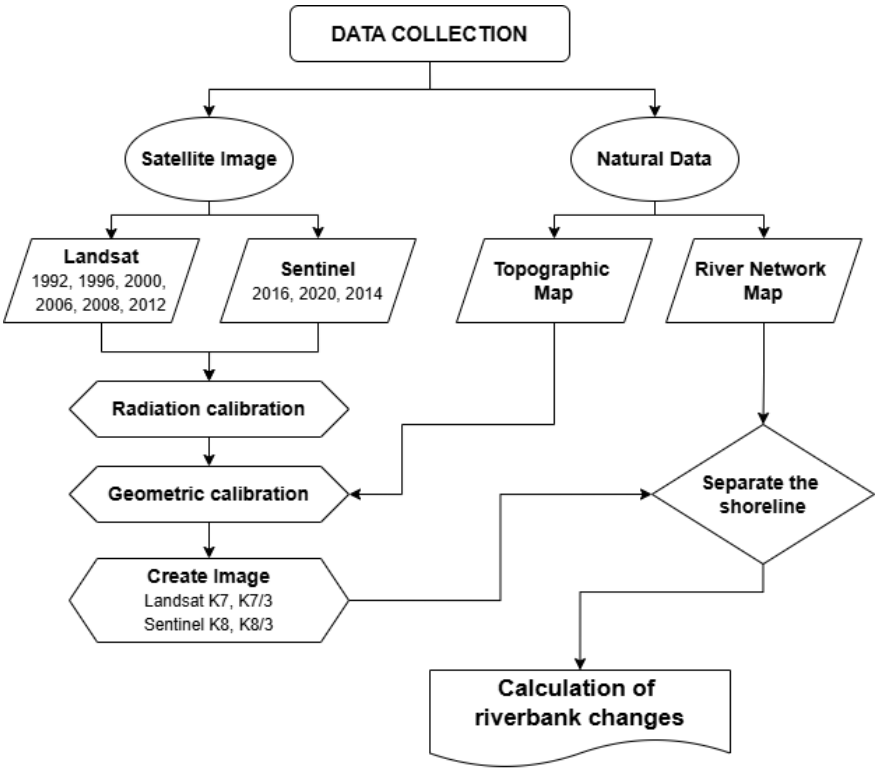

b) Calculation of shoreline change indicators:

Three main indicators were used to quantify shoreline dynamics:

- End Point Rate (EPR): This index measures the rate of shoreline change by calculating the ratio between shoreline displacement and the time interval from 1992 to 2024. It reflects the magnitude of change between two specific time points and provides a direct estimate of short-term shoreline movement.
- Linear Regression Rate (LRR): This indicator evaluates the average rate of shoreline change using linear regression analysis based on shoreline positions derived from multiple time periods. The method enables the identification of long-term trends while minimizing the influence of short-term fluctuations or anomalous events.
- Shoreline Change Envelope (SCE): This metric represents the maximum range of shoreline variability by measuring the distance between the most landward and most seaward shoreline positions at each transect within the study area.

Together, these indicators provide a comprehensive assessment of shoreline variability and long-term coastal dynamics.

2.3 Database

Landsat imagery: Downloaded from the website of the United States Geological Survey, these datasets provide medium-resolution satellite data suitable for long-term monitoring and analysis of riverbank dynamics (Table 1).

Sentinel imagery: Obtained from the Copernicus Programme website of the European Union, Sentinel images offer higher spatial resolution, enabling more detailed monitoring of recent shoreline changes (Table 1).

Table 1

Database for monitoring shoreline dynamics in An Giang Province

Year	**Data**	**Number**
1992	LT05_L2SP_125053_19920125_20200914_02_T1 LT05_L2SP_126052_19920421_20200915_02_T1	2
1996	LT05_L2SP_125053_19960324_20200911_02_T1 LT05_L2SP_126052_19960603_20200911_02_T1	2
2000	LT05_L2SP_125053_20000927_20200906_02_T1 LT05_L2SP_126052_20000427_20200907_02_T1	2
2004	LT05_L2SP_125053_20041211_20200902_02_T1 LT05_L2SP_126052_20041218_20200902_02_T1	2
2008	LT05_L2SP_125053_20080325_20200829_02_T1 LT05_L2SP_126052_20080401_20200829_02_T1	2
2012	LE07_L2SP_125053_20121225_20200908_02_T1 LE07_L2SP_126052_20121216_20200908_02_T1	2
2016	T48PWS_20160206T033242	1
2020	T48PWS_20200430T031539	1
2024	T48PWS_20240320T031519	1
	Total	**15**

The satellite imagery database used for shoreline analysis is summarized in Table 1, which includes multi-temporal Landsat and Sentinel-2 datasets acquired between 1992 and 2024. These datasets provide a consistent temporal record for monitoring long-term riverbank dynamics in An Giang Province. Based on the extracted shorelines from these satellite images, eight representative river reaches were selected for detailed analysis, as listed in Table 2. The selected segments range from 1.38 to 1.96 km in length and are distributed across key riverbank areas such as Tan Chau, Phu Tan, and Chau Phu, where

significant bank instability and morphological changes have been observed. The spatial distribution of these study reaches is illustrated in Figure 2, which provides a geographic overview of the monitoring locations along the river system. Together, Table 1, Table 2, and Figure 2 present the integrated data framework used in this study, linking the satellite data sources, the selected monitoring segments, and their spatial distribution within the study area.

Table 2

Typical river reaches selected for analysis

No.	Code	Length (m)	Location
1	VT1	1,540	Tan An – Tan Chau area
2	VT2	1,380	Cai Vung – Phu Tan area
3	VT3	1,680	Chau Phong – Tan Chau area
4	VT4	1,580	Phu An – Phu Tan area
5	VT5	1,920	Hanh Trung, Cai Dau – Chau Phu
6	VT6	1,600	Con Binh Thuy – Chau Phu
7	VT7	1,760	Long Dien A area
8	VT8	1,960	Hoa An area

3 RESULT AND DISCUSSION

Results of shoreline change analysis: The Digital Shoreline Analysis System (DSAS) was used to calculate the extent and distance of riverbank erosion within the study area across nine key observation years: 1992, 1996, 2000, 2004, 2008, 2012, 2016, 2020, and 2024. By applying the DSAS framework, a series of transects perpendicular to the shoreline were generated, enabling the measurement of shoreline displacement and the assessment of spatial variability over time. This approach allowed for the accurate estimation of land area lost due to erosion as well as the magnitude of shoreline retreat at each observation period, thereby providing important quantitative data for evaluating the trends and severity of erosion throughout the study period.

3.1 Calculation of the average shoreline change rate (LRR index)

The results of the average shoreline change rate, calculated using the Linear Regression Rate (LRR) indicator, for the eight surveyed river segments are presented in Figure 3 and Table 3. The LRR values were derived through linear regression analysis based on shoreline positions obtained from multiple observation years. The analysis reveals considerable spatial variability in shoreline change rates among the investigated segments, indicating that riverbank dynamics are not uniform across the study area. In particular, some reaches exhibit pronounced erosion trends, while others show relatively stable conditions or localized accretion. These variations highlight the heterogeneous nature of riverbank processes and provide important insights into the spatial patterns of shoreline instability within the study region.

Figure 3

Average shoreline variation over the years across the eight studied river reaches

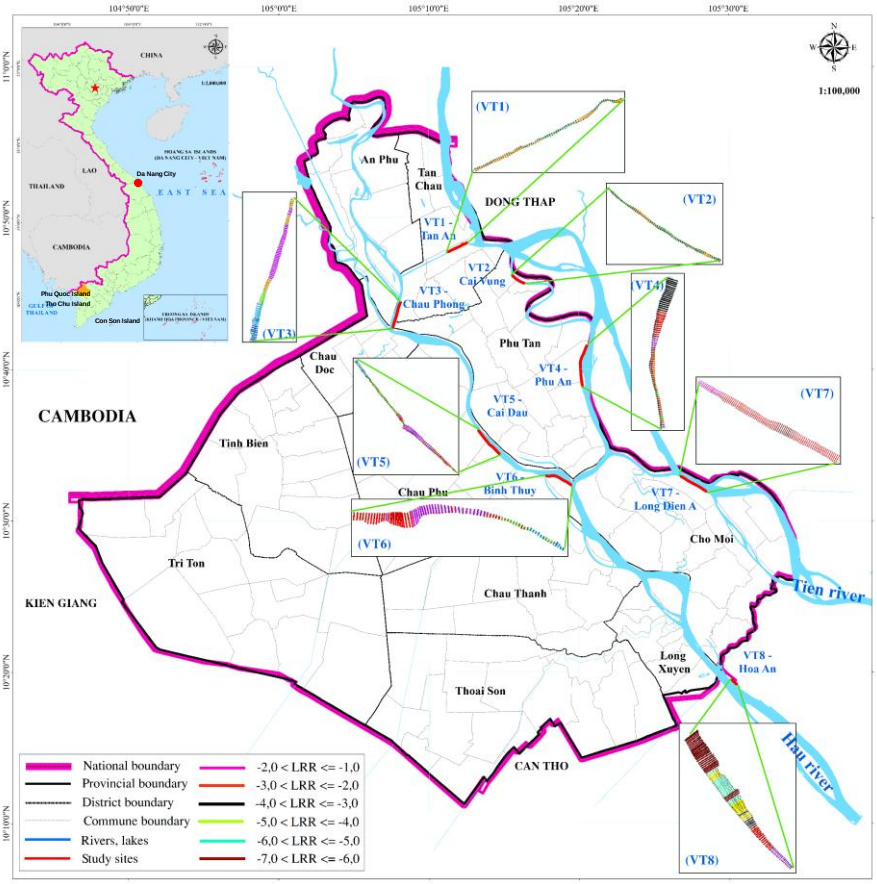

Table 3

Results of the average shoreline change rate calculated using the Linear Regression Rate (LRR) index

Surveyed segment	LRR (m/year)	Number of transects	Distance (m)	Proportion (%)	Condition assessment	Proportion (%)
VT1	-0,5 < LRR ≤ 0	31	620	40.26	Erosion	100
	-1,0 < LRR ≤ -0,5	46	920	59.74	Erosion	
	Total	**77**	**1,540**	**100**		
VT2	-0,5 < LRR ≤ 0	51	1020	73.91	Erosion	97,1
	-1,0 < LRR ≤ -0,5	16	320	23.19	Erosion	
	0 < LRR ≤ 0,5	2	40	2.90	Accretion	2,9
	Total	**69**	**1,380**	**100**		
VT3	1,0 < LRR ≤ 2,0	2	40	2.50	Accretion	25,1
	0,5 < LRR ≤ 1,0	9	180	10.70	Accretion	
	0 < LRR ≤ 0,5	10	200	11.90	Accretion	
	-0,5 < LRR ≤ 0	7	140	8.33	Erosion	74,9
	-1,0 < LRR ≤ -0,5	18	360	21.43	Erosion	
	-2,0 < LRR ≤ -1,0	38	760	45.23	Erosion	
	Total	**84**	**1,680**	**100**		
VT4	-0,5 < LRR ≤ 0	4	80	5.06	Erosion	100
	-1,0 < LRR ≤ -0,5	34	680	43.04	Erosion	
	-2,0 < LRR ≤ -1,0	9	180	11.39	Erosion	
	-3,0 < LRR ≤ -2,0	14	280	17.73	Erosion	
	-4,0 < LRR ≤ -3,0	18	360	22.78	Erosion	
	Total	**79**	**1,580**	**100**		
VT5	0 < LRR ≤ 0,5	15	300	15.62	Accretion	0,81
	-0,5 < LRR ≤ 0	34	680	35.42	Erosion	99,19
	-1,0 < LRR ≤ -0,5	26	520	27.08	Erosion	
	-2,0 < LRR ≤ -1,0	21	420	21.88	Erosion	
	Total	**96**	**1,920**	**100**		
VT6	0,5 < LRR ≤ 1,0	1	20	1.25	Accretion	13,75
	0 < LRR ≤ 0,5	10	200	12.5	Accretion	
	-0,5 < LRR ≤ 0	12	240	15.00	Erosion	86,25
	-1,0 < LRR ≤ -0,5	32	640	40.00	Erosion	
	-2,0 < LRR ≤ -1,0	25	500	31.25	Erosion	
	Total	**80**	**1,600**	**100**		
VT7	-4,0 < LRR ≤ -3,0	11	220	12.50	Erosion	100
	-3,0 < LRR ≤ -2,0	62	1240	70.45	Erosion	
	-2,0 < LRR ≤ -1,0	15	300	17.05	Erosion	
	Total	**88**	**1,760**	**100**		
VT8	-2,0 < LRR ≤ -1,0	16	320	16.33	Erosion	100
	-3,0 < LRR ≤ -2,0	15	300	15.30	Erosion	
	-4,0 < LRR ≤ -3,0	6	120	6.12	Erosion	
	-5,0 < LRR ≤ -4,0	16	320	16.33	Erosion	
	-6,0 < LRR ≤ -5,0	16	320	16.33	Erosion	
	-7,0 < LRR ≤ -6,0	29	580	29.59	Erosion	
	Total	**98**	**1,960**	**100**		

Within the 14 km riverbank reach investigated, the study area was divided into eight survey segments (VT1–VT8) (see Figure 3). Each segment has a length ranging

from approximately 1.7 to 2.1 km depending on the observation period. Analysis of riverbank dynamics between 1992 and 2024 reveals that erosion is the dominant geomorphic process along most of the study reach. Severe erosion hotspots were identified at segments VT4, VT7, and VT8, whereas limited accretion occurred locally at VT2, VT3, VT5, and VT6 but represented only a small proportion of the total riverbank length.

At VT1, all 77 surveyed transects experienced erosion, representing 100% of the monitored riverbank length. Slight erosion rates of 0–0.5 m yr^{-1} ($-0.5 < LRR \leq 0$) accounted for 40.26%, while moderate erosion rates of 0.5–1.0 m yr^{-1} ($-1.0 < LRR \leq -0.5$) represented 59.74%. A similar pattern was observed at VT2, where erosion dominated 97.1% of the segment. Slight erosion accounted for 73.91% of the riverbank, while moderate erosion accounted for 23.19%. Only 2.9% of the riverbank exhibited slight accretion ($0 < LRR \leq 0.5$ m yr^{-1}).

Segment VT3 showed a more heterogeneous pattern, with erosion affecting 74.9% of the riverbank and accretion accounting for 25.1%. Strong erosion rates of 1–2 m yr^{-1} ($-2.0 < LRR \leq -1.0$) dominated this segment, representing 45.23% of the riverbank length, while accretion mainly occurred at slight to moderate levels (0–2 m yr^{-1}).

Erosion intensity increased markedly in the downstream segments. At VT4, erosion affected the entire monitored riverbank (100%), with strong (2–3 m yr^{-1}) and very strong (3–4 m yr^{-1}) erosion accounting for 17.73% and 22.78% of the riverbank length, respectively. Similarly, VT5 experienced predominantly erosional conditions (99.19%), with moderate to strong erosion rates together accounting for nearly half of the riverbank length. Accretion was minimal, representing only 0.81% of the segment.

At VT6, erosion occurred along 86.25% of the riverbank, mainly at moderate to strong levels (71.25%), while accretion accounted for 13.75% and was largely limited to slight and moderate deposition (0–1 m yr^{-1}). In contrast, VT7 exhibited pervasive erosion across the entire segment, with strong erosion (2–3 m yr^{-1}) dominating 70.45% of the riverbank and very strong erosion (3–4 m yr^{-1}) accounting for 12.50%.

Among all surveyed segments, VT8 experienced the most severe riverbank instability. Erosion affected 100% of the monitored riverbank, with extremely high erosion rates reaching 6–7 m yr^{-1} at several locations. This class alone represented 29.59% of the segment, indicating rapid bank retreat and intense morphological change.

Overall, the spatial distribution of erosion intensity suggests that channel morphology and local hydrodynamic conditions play a critical role in controlling riverbank stability along the study reach. The severe erosion observed at VT4, VT7, and particularly VT8 is likely associated with zones of strong flow concentration and channel curvature, where secondary currents enhance near-bank shear stress. In contrast, the limited accretion detected at VT2, VT3, VT5, and VT6 may reflect localized sediment deposition in relatively low-energy zones, such as inner bends or sections with reduced flow velocity. These findings highlight the strong coupling between river hydrodynamics, sediment transport processes, and channel planform evolution in driving long-term riverbank dynamics.

3.2 Instantaneous shoreline change analysis using the EPR index

The instantaneous shoreline change rate calculated using the End Point Rate (EPR) indicates that erosion is the dominant geomorphic process across all surveyed river segments. As illustrated in Figure 4 and quantified in Table 4, the majority of transects show negative EPR values, confirming widespread riverbank retreat along the study reach during the observation period. Particularly severe erosion was recorded at segments VT4, VT7, and VT8, where strong to very strong erosion classes account for a large proportion of the monitored riverbank length. In contrast, accretion processes were only locally observed in segments VT2, VT3, VT5, and VT6, and mainly occurred at slight deposition levels.

At segment VT1, erosion affected the entire monitored riverbank. As shown in Table 4, moderate erosion rates ranging from −0.5 to 0 m yr^{-1} accounted for 48.05% of the surveyed transects, while higher erosion rates between −1.0 and −0.5 m yr^{-1} represented 50.65%. This pattern indicates relatively uniform but persistent bank retreat along the segment.

Figure 4

Instantaneous shoreline variation across the eight studied river reaches

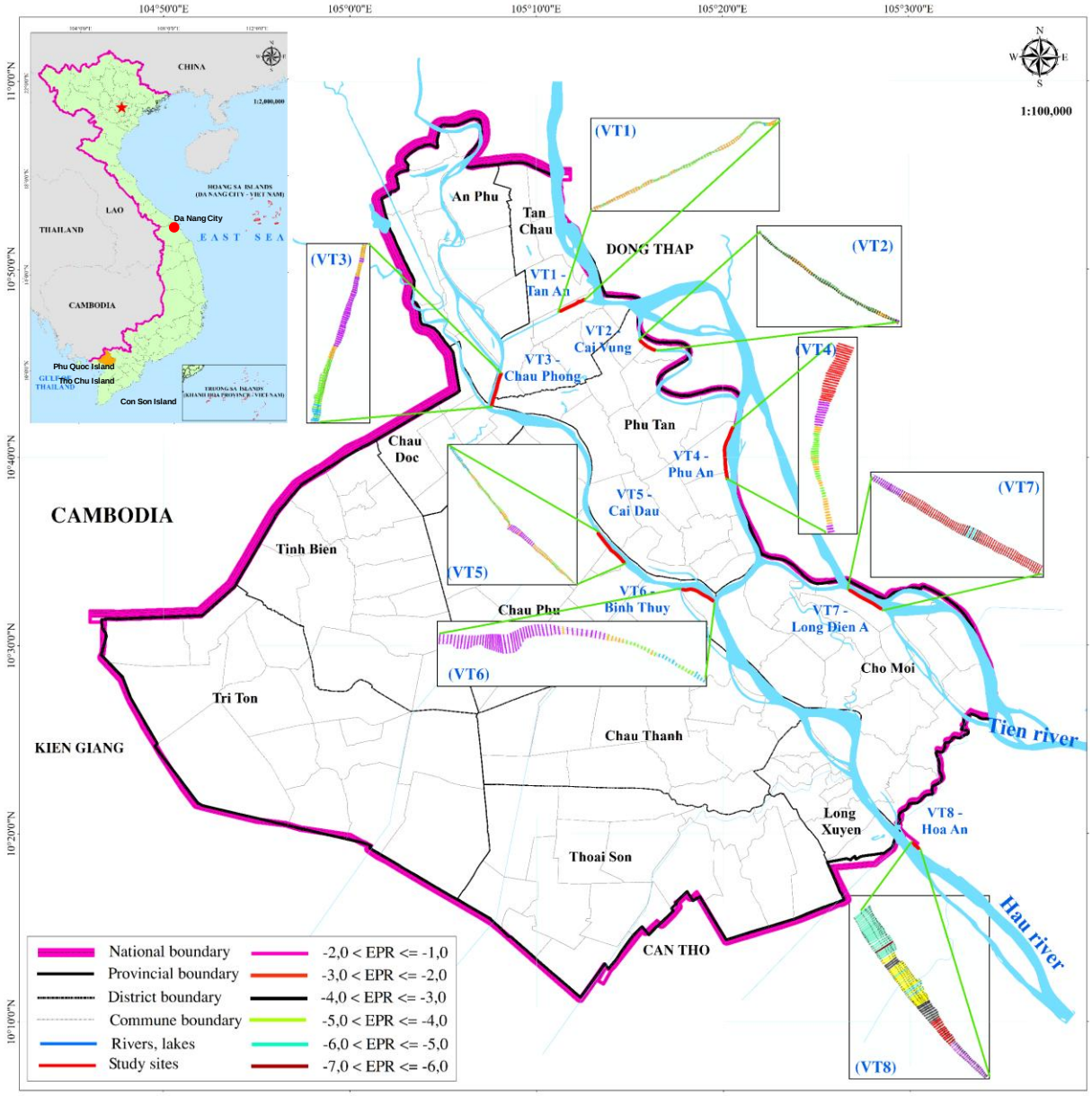

Table 4

Results of the instantaneous shoreline change rate calculated using the End Point Rate (EPR) index

Surveyed segment	EPR (m/year)	Number of transects	Distance (m)	Proportion (%)	Conclusion	Proportion (%)
VT1	0 < EPR ≤ 0,5	1	20	1.30	Erosion	100
	-0,5 < EPR ≤ 0	37	740	48.05	Erosion	
	-1,0 < EPR ≤ -0,5	39	780	50.65	Erosion	
	Total	**77**	**1,540**	**100**		
VT2	-0,5 < EPR ≤ 0	53	1.060	76.81	Erosion	89,85
	-1,0 < EPR ≤ -0,5	9	180	13.04	Erosion	
	0 < EPR ≤ 0,5	7	140	10.15	Accretion	10,15
	Total	**69**	**1,380**	**100**		
VT3	0 < LRR ≤ 0,5	6	120	7.14	Accretion	7,14
	-0,5 < LRR ≤ 0	22	440	26.19	Erosion	92,86
	-1,0 < LRR ≤ -0,5	19	380	22.62	Erosion	
	-2,0 < LRR ≤ -1,0	37	740	44.05	Erosion	
	Total	**84**	**1,680**	**100**		
VT4	-0,5 < LRR ≤ 0	21	420	26.58	Erosion	100
	-1,0 < LRR ≤ -0,5	20	400	25.32	Erosion	
	-2,0 < LRR ≤ -1,0	13	260	16.46	Erosion	
	-3,0 < LRR ≤ -2,0	25	500	31.64	Erosion	
	Total	**79**	**1,580**	**100**		
VT5	0 < EPR ≤ 0,5	15	300	15.62	Accretion	15,62
	-0,5 < EPR ≤ 0	35	700	36.46	Erosion	83,38
	-1,0 < EPR ≤ -0,5	30	600	31.25	Erosion	
	-2,0 < EPR ≤ -1,0	16	320	16.67	Erosion	
	Total	**96**	**1,920**	**100**		
VT6	0 < EPR ≤ 0,5	10	200	12.5	Accretion	12,5
	-0,5 < EPR ≤ 0	13	260	16.25	Erosion	87,5
	-1,0 < EPR ≤ -0,5	7	140	8.75	Erosion	
	-2,0 < EPR ≤ -1,0	50	1,000	62.5	Erosion	
	Total	**80**	**1,600**	**100**		
VT7	-4,0 < EPR ≤ -3,0	8	160	9.09	Erosion	100
	-3,0 < EPR ≤ -2,0	64	1,280	72.73	Erosion	
	-2,0 < EPR ≤ -1,0	16	320	18.18	Erosion	
	Total	**88**	**1,760**	**100**		
VT8	-2,0 < EPR ≤ -1,0	22	440	22.45	Erosion	100
	-3,0 < EPR ≤ -2,0	12	240	12.24	Erosion	
	-4,0 < EPR ≤ -3,0	12	240	12.24	Erosion	
	-5,0 < EPR ≤ -4,0	22	440	22.45	Erosion	
	-6,0 < EPR ≤ -5,0	29	580	29.59	Erosion	
	-7,0 < EPR ≤ -6,0	1	20	1.03	Erosion	
	Total	**98**	**1,960**	**100**		

Segment VT2 also exhibited predominantly erosional conditions, with 89.85% of the transects characterized by negative EPR values. Slight erosion ($-0.5 < EPR \leq 0$) accounted for 76.81% of the riverbank length, while moderate erosion ($-1.0 < EPR \leq$

−0.5) represented 13.04%. Only 10.15% of the transects showed slight accretion, indicating localized sediment deposition under relatively low-energy conditions.

At VT3, erosion remained the dominant process (92.86%), although minor accretion occurred at several transects. The most common erosion class was $-2.0 < EPR \leq -1.0$ m yr^{-1}, accounting for 44.05% of the riverbank length, suggesting stronger erosional dynamics compared with upstream segments.

The erosion intensity increases further at segment VT4, where all transects recorded negative EPR values. Strong erosion rates between −3.0 and −2.0 m yr^{-1} accounted for 31.64% of the riverbank length, while moderate erosion classes also contributed significantly. This indicates a highly unstable riverbank environment characterized by active lateral channel migration.

Segments VT5 and VT6 exhibit mixed dynamics but remain predominantly erosional. At VT5, erosion accounted for 83.38% of the transects, with the most frequent classes being $-0.5 < EPR \leq 0$ (36.46%) and $-1.0 < EPR \leq -0.5$ (31.25%). Slight accretion (15.62%) occurred locally, suggesting the presence of depositional zones along inner-bank areas or areas with reduced flow velocity. At VT6, erosion dominated 87.5% of the riverbank, with the class $-2.0 < EPR \leq -1.0$ m yr^{-1} accounting for the largest proportion (62.5%), indicating relatively high erosion intensity within this segment.

The most severe erosion conditions were recorded in the downstream segments VT7 and VT8. At VT7, erosion affected 100% of the monitored riverbank, with strong erosion rates between −3.0 and −2.0 m yr^{-1} dominating (72.73%). At VT8, erosion intensity reached the highest levels observed in the study area, with multiple transects showing erosion rates exceeding −4 m yr^{-1}. The most frequent class was $-6.0 < EPR \leq -5.0$ m yr^{-1}, representing 29.59% of the riverbank length, indicating extremely rapid bank retreat and significant morphological instability.

The spatial distribution of EPR values reveals a clear downstream increase in erosion intensity, particularly from VT4 to VT8. The patterns observed in Figure 5 and Table 4 suggest that riverbank instability is strongly influenced by local hydrodynamic conditions, including flow concentration, channel curvature, and sediment transport dynamics. Segments experiencing the highest erosion rates likely correspond to zones where secondary flow and near-bank shear stress are intensified, accelerating lateral channel migration and bank collapse. Conversely, the limited accretion detected in some

upstream segments may reflect localized sediment deposition in relatively low-energy environments.

3.3 Shoreline change envelope analysis using the SCE index

The shoreline change envelope calculated using the Shoreline Change Envelope (SCE) provides an estimate of the maximum spatial extent of shoreline movement during the study period. The results reveal substantial spatial variability in shoreline displacement across the eight surveyed river segments. As illustrated in Figure 5 and summarized in Table 5, the largest shoreline displacement occurred in segments VT7 and VT8, where the SCE values exceed 100 m at many transects and locally reach up to 200 m. In contrast, segments VT1, VT2, and VT5 exhibit relatively smaller shoreline movement, generally below 30 m, indicating comparatively stable riverbank conditions.

At segment VT1, shoreline displacement is relatively limited, with most transects falling within the range of $10 < SCE \leq 20$ m, accounting for 62.34% of the monitored riverbank length. An additional 35.06% of the transects fall within the range of $20 < SCE \leq 30$ m. These results indicate moderate but relatively uniform shoreline adjustments along the segment.

A similar pattern is observed at VT2, where shoreline displacement is concentrated within the ranges of 10–20 m (59.42%) and 20–30 m (34.78%). The limited SCE values in this segment suggest relatively stable channel morphology with minor lateral migration during the observation period.

Figure 5

Shoreline change envelope across the eight studied river reaches

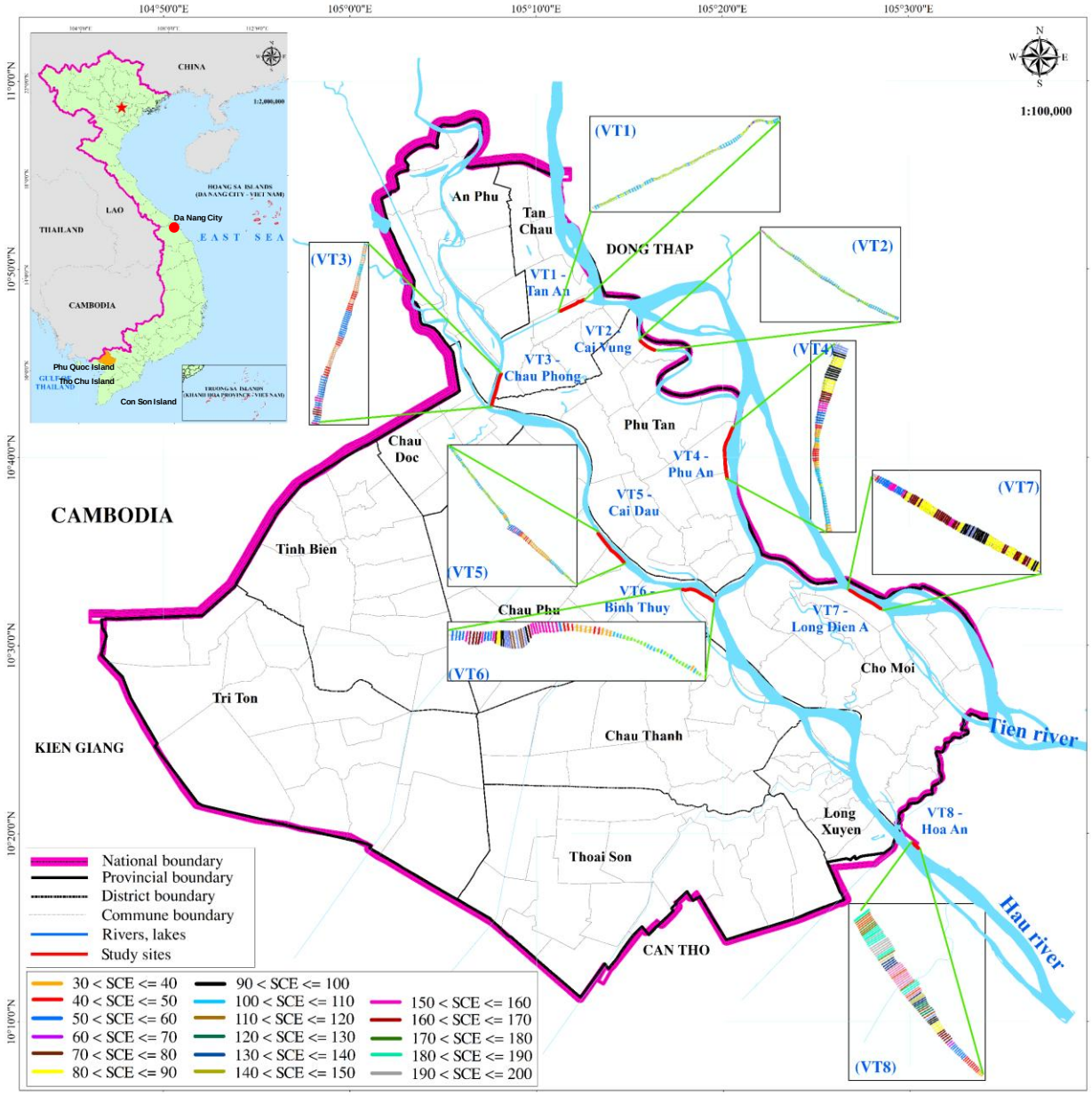

Table 5

Results of shoreline change envelope calculations (SCE index)

Survey location	SCE (m/year)	Number of transects	Distance (m)	Proportion (%)
VT1	0 < SCE ≤ 10	2	20	2.6
	10 < SCE ≤ 20	48	960	62.34
	20 < SCE ≤ 30	27	540	35.06
	Total	**77**	**1,540**	**100**
VT2	0 < SCE ≤ 10	4	80	5.80
	10 < SCE ≤ 20	41	820	59.42
	20 < SCE ≤ 30	24	480	34.78
	Total	**69**	**1,380**	**100**
VT3	20 < SCE ≤ 30	8	160	9.52
	30 < SCE ≤ 40	26	520	30.95
	40 < SCE ≤ 50	16	320	19.05
	50 < SCE ≤ 60	27	540	32.14
	60 < SCE ≤ 70	4	80	4.76
	70 < SCE ≤ 80	3	60	3.57
	Total	**84**	**1,680**	**100**
VT4	10 < SCE ≤ 20	1	20	1.27
	20 < SCE ≤ 30	23	460	29.11
	30 < SCE ≤ 40	13	260	16.46
	40 < SCE ≤ 50	8	160	10.13
	50 < SCE ≤ 60	5	100	6.33
	60 < SCE ≤ 70	4	80	5.06
	70 < SCE ≤ 80	5	100	6.33
	80 < SCE ≤ 90	9	180	11.40
	90 < SCE ≤ 100	8	160	10.13
	100 < SCE ≤ 110	3	60	3.80
	Total	**79**	**1,580**	**100**
VT5	10 < SCE ≤ 20	33	660	34.38
	20 < SCE ≤ 30	33	660	34.38
	30 < SCE ≤ 40	18	360	18.75
	40 < SCE ≤ 50	5	100	5.20
	50 < SCE ≤ 60	6	120	6.25
	60 < SCE ≤ 70	1	20	1.04
	Total	**96**	**1,920**	**100**
VT6	10 < SCE ≤ 20	17	340	21.25
	20 < SCE ≤ 30	10	200	12.5
	30 < SCE ≤ 40	8	160	10
	40 < SCE ≤ 50	5	100	6.25
	50 < SCE ≤ 60	8	160	10
	60 < SCE ≤ 70	12	240	15
	70 < SCE ≤ 80	6	120	7.5
	80 < SCE ≤ 90	2	40	2.5
	90 < SCE ≤ 100	3	60	3.75
	100 < SCE ≤ 110	5	100	6.25
	110 < SCE ≤ 120	4	80	5
	Total	**80**	**1,600**	**100**
VT7	40 < SCE ≤ 50	1	20	1.14
	50 < SCE ≤ 60	10	200	11.36
	60 < SCE ≤ 70	7	140	7.95
	70 < SCE ≤ 80	25	500	28.41

Survey location	SCE (m/year)	Number of transects	Distance (m)	Proportion (%)
	80 < SCE ≤ 90	30	600	34.09
	90 < SCE ≤ 100	13	260	14.77
	100 < SCE ≤ 110	2	40	2.27
	Total	**88**	**1,760**	**100**
VT8	30 < SCE ≤ 40	3	60	3.06
	40 < SCE ≤ 50	9	180	9.18
	50 < SCE ≤ 60	8	160	8.16
	60 < SCE ≤ 70	2	40	2.04
	70 < SCE ≤ 80	6	120	6.12
	80 < SCE ≤ 90	4	80	4.08
	90 < SCE ≤ 100	3	60	3.06
	100 < SCE ≤ 110	1	20	1.02
	110 < SCE ≤ 120	2	40	2.04
	120 < SCE ≤ 130	5	100	5.1
	130 < SCE ≤ 140	7	140	7.14
	140 < SCE ≤ 150	4	80	4.08
	150 < SCE ≤ 160	12	240	12.24
	160 < SCE ≤ 170	6	120	6.12
	170 < SCE ≤ 180	6	120	6.12
	180 < SCE ≤ 190	14	280	14.29
	190 < SCE ≤ 200	6	120	6.12
	Total	**98**	**1,960**	**100**

In contrast, segment VT3 exhibits substantially larger shoreline displacement. The most dominant classes occur within the ranges of 30–40 m (30.95%) and 50–60 m (32.14%), indicating more pronounced bank migration compared with upstream segments. This suggests active channel adjustment and enhanced bank erosion processes within this reach.

Segment VT4 shows a wide range of SCE values, reflecting heterogeneous shoreline dynamics. Although the largest proportion of transects occurs within the range of 20–30 m (29.11%), several transects show displacement exceeding 80 m, with the class 80–90 m accounting for 11.40%. This wide distribution indicates localized zones of intense bank retreat associated with dynamic channel adjustment.

At VT5, shoreline displacement remains relatively moderate. The majority of transects fall within the ranges of 10–20 m and 20–30 m, which together account for 68.76% of the monitored riverbank length. These values suggest relatively stable shoreline conditions with limited large-scale channel migration.

Segment VT6 exhibits a broader distribution of shoreline displacement values. The ranges from 10 to 70 m account for approximately 64.5% of the transects, while

several locations exceed 100 m. This pattern indicates moderate to high variability in bank dynamics, suggesting localized erosion hotspots within the segment.

The most significant shoreline displacement occurs in the downstream segments VT7 and VT8. At VT7, the dominant classes are 80–90 m (34.09%) and 70–80 m (28.41%), reflecting strong lateral channel migration and extensive bank retreat. Meanwhile, VT8 exhibits the largest shoreline displacement across the entire study area. Several transects show SCE values exceeding 150 m, with the ranges of 180–190 m (14.29%) and 150–160 m (12.24%) representing the most common classes. These extremely high values indicate substantial riverbank instability and rapid morphological adjustment.

The spatial pattern of SCE values reveals a clear increase in shoreline displacement from upstream to downstream segments. The large SCE values observed at VT7 and VT8 indicate zones of intense channel migration and morphological instability. These areas likely correspond to sections of the river characterized by strong hydrodynamic forcing, channel curvature, and enhanced near-bank shear stress. Conversely, the relatively small SCE values recorded at VT1, VT2, and VT5 suggest more stable channel conditions with limited lateral migration. The combined interpretation of SCE patterns and EPR-derived erosion rates therefore provides a comprehensive understanding of riverbank dynamics, highlighting critical hotspots of erosion and channel adjustment within the study reach.

4 DISCUSSION

4.1 Spatial patterns of riverbank change derived from multi-temporal remote sensing

The results obtained from the End Point Rate (EPR), Net Shoreline Movement (NSM), and Shoreline Change Envelope (SCE) analyses reveal that erosion is the dominant morphodynamic process along the investigated river sections, while accretion occurs locally and at relatively lower magnitudes. This spatial pattern indicates a net negative sediment balance and strong bank instability, particularly at locations VT4, VT7, and VT8 where erosion intensity is significantly higher than in other segments.

The consistency between the three DSAS indicators (EPR, NSM, and SCE) suggests that the observed riverbank migration is not only episodic but represents a persistent geomorphic trend. Similar relationships between erosion-dominated shoreline change and river morphodynamics have been reported in other river and coastal systems analyzed using remote sensing techniques. For example, Bheeroo et al. (2016) demonstrated that DSAS-derived shoreline metrics provide robust quantitative evidence of long-term erosion trends along the northwest coast of Mauritius. Likewise, Al-Zubieri et al. (2020) and Alharbi et al. (2023) confirmed that multi-temporal satellite imagery combined with DSAS analysis is effective in detecting spatially heterogeneous shoreline dynamics in sediment-limited environments.

In the present study area, the strongest erosion zones correspond to river bends and high-curvature channel segments, suggesting that lateral channel migration driven by hydrodynamic forces plays a key role in bank retreat. High flow velocity along the outer banks of meanders increases shear stress and promotes bank undercutting, while sediment deposition tends to occur along the inner banks. This pattern is consistent with classical fluvial morphodynamics and has been widely documented in riverbank erosion studies using geospatial methods (Bordoloi et al., 2020).

4.2 Hydrodynamic controls and sediment supply influencing erosion patterns

The spatial variability of shoreline change observed in this study is strongly related to hydrodynamic conditions, sediment transport processes, and channel morphology. The severe erosion observed at sites VT4, VT7, and VT8 can be interpreted as the result of concentrated flow energy combined with reduced bank resistance, which accelerates lateral channel migration.

Riverbank erosion is often intensified when sediment supply decreases or when flow energy exceeds the threshold required to mobilize bank materials. In large deltaic systems such as the Mekong Delta, upstream hydrological regulation and sediment trapping by reservoirs have been reported to significantly reduce sediment delivery to downstream reaches, thereby enhancing erosion processes (Binh et al., 2020). Reduced sediment availability limits natural bank replenishment and promotes channel widening, which may partly explain the erosion-dominated trend observed in the present study.

Additionally, extreme hydrological events and seasonal discharge fluctuations may amplify bank instability by increasing hydraulic pressure and triggering bank collapse. Previous studies have highlighted that riverbank erosion in deltaic environments is often associated with extreme weather events and hydrological variability (Abdel Aziz, 2024). Therefore, the erosion patterns detected in this study likely reflect a combined effect of long-term hydrological change and local geomorphological conditions.

4.3 Comparison with previous remote sensing studies

The magnitude and spatial distribution of shoreline change identified in this study are broadly consistent with findings from other remote sensing-based shoreline monitoring studies. For instance, Boak and Turner (2005) emphasized that accurate shoreline detection and multi-temporal satellite imagery are essential for capturing long-term coastal and riverbank dynamics. The present study confirms that Landsat-derived shoreline datasets combined with DSAS analysis provide reliable indicators of riverbank change over decadal timescales.

In the Mekong Delta context, Binh et al. (2020) proposed a novel Landsat-based approach for detecting riverbanks and monitoring morphological changes, highlighting the importance of satellite data in large-scale erosion monitoring. Compared with that study, the present research further extends the application of remote sensing by integrating multiple shoreline change indicators (EPR, NSM, and SCE) to quantify erosion intensity and spatial variability along specific river segments. This multi-indicator approach provides a more comprehensive understanding of bank dynamics and improves the reliability of erosion risk assessment.

Similarly, studies in other regions such as the Red Sea coast (Al-Zubieri et al., 2020; Alharbi et al., 2023) and the Subansiri River in India (Bordoloi et al., 2020) have demonstrated that DSAS-based metrics can effectively quantify shoreline migration and identify erosion hotspots. However, most of these studies focus primarily on coastal shorelines, whereas the present research applies similar analytical frameworks to riverbank environments within a complex deltaic system, highlighting the adaptability of DSAS for fluvial geomorphological investigations.

4.4 Scientific contribution and novelty of the study

The results of this study contribute to the growing body of research on remote sensing-based monitoring of riverbank erosion in deltaic environments. Several aspects highlight the novelty and scientific contribution of the present work.

First, the study provides a systematic multi-indicator assessment of riverbank dynamics using EPR, NSM, and SCE indices, allowing for a detailed characterization of both erosion intensity and spatial variability along the river system.

Second, the integration of multi-temporal satellite imagery with morphodynamic interpretation enables the identification of erosion hotspots associated with channel curvature and hydrodynamic forcing. This approach enhances the understanding of the physical processes driving riverbank instability in the study area.

Third, the findings provide important baseline data for developing erosion early-warning systems, particularly in the context of increasing hydrological variability and extreme weather conditions. The quantitative shoreline change indicators derived from remote sensing data can serve as key inputs for artificial intelligence–based erosion prediction models, which is consistent with the broader objective of the research project supporting this study.

Overall, the study demonstrates that satellite remote sensing combined with DSAS analysis represents a powerful tool for monitoring riverbank evolution, identifying erosion-prone areas, and supporting sustainable river management strategies in vulnerable delta regions.

5 CONCLUSION

This study applied multi-temporal satellite imagery and the Digital Shoreline Analysis System (DSAS) to quantify riverbank dynamics and identify erosion hotspots along the investigated river sections in An Giang Province, Vietnam. By integrating three shoreline change indicators: End Point Rate (EPR), Net Shoreline Movement (NSM), and Shoreline Change Envelope (SCE), the research provides a comprehensive assessment of spatial and temporal riverbank variations and their underlying morphodynamic controls.

1. The results indicate that riverbank erosion is the dominant geomorphological process across most of the investigated sections, with particularly severe erosion observed at locations VT4, VT7, and VT8. The EPR analysis shows that high and very high erosion rates occur frequently in these segments, while accretion is limited and mainly concentrated at VT2, VT3, VT5, and VT6 with relatively low magnitudes. The NSM and SCE results further confirm that shoreline retreat has occurred persistently over the study period, suggesting long-term bank instability rather than short-term fluctuations.
2. The spatial distribution of erosion and accretion patterns reveals a strong relationship with channel curvature, hydrodynamic conditions, and sediment transport processes. Severe erosion tends to occur along outer bends and high-curvature river segments where flow velocity and shear stress are concentrated, promoting bank undercutting and lateral channel migration. In contrast, accretion zones are generally located along inner bends where flow energy decreases and sediment deposition occurs. These findings highlight the important role of fluvial morphodynamics in controlling riverbank evolution in deltaic environments.
3. From a scientific perspective, this study contributes to the growing field of remote sensing–based riverbank monitoring in several ways. First, it demonstrates the effectiveness of combining multi-temporal satellite data with DSAS-based shoreline metrics to quantify riverbank change at a regional scale. Second, the integration of multiple shoreline change indicators (EPR, NSM, and SCE) allows for a more robust interpretation of erosion intensity and spatial variability compared with single-indicator approaches. Third, the identification of erosion hotspots provides important baseline information for riverbank management and the development of early warning systems for erosion hazards, particularly in the context of increasing hydrological variability and extreme weather events in the Mekong Delta region.

Despite these contributions, several limitations should be acknowledged. The shoreline extraction was based primarily on medium-resolution satellite imagery, which may introduce positional uncertainties in shoreline delineation, particularly in areas with dense vegetation or complex bank morphology. In addition, the DSAS analysis focuses on geometric shoreline changes and does not directly incorporate hydrodynamic

parameters such as flow velocity, sediment load, or bank material properties. These factors may significantly influence erosion processes but were beyond the scope of the present study.

Future research should therefore focus on integrating higher-resolution remote sensing data (e.g., UAV imagery, LiDAR, or high-resolution satellite datasets) with hydrodynamic and sediment transport models to improve the accuracy of riverbank change detection and process interpretation. In addition, combining remote sensing–derived shoreline change indicators with machine learning or artificial intelligence techniques may provide new opportunities for developing predictive models and real-time early warning systems for riverbank erosion. Such approaches would significantly enhance the capacity for sustainable river management and hazard mitigation in vulnerable deltaic environments.

Overall, the findings of this study demonstrate that remote sensing combined with DSAS analysis provides a powerful and cost-effective tool for long-term monitoring of riverbank dynamics, offering valuable insights for both scientific research and practical riverbank management in rapidly changing delta systems.

AUTHOR CONTRIBUTIOSN

Conceptualisation, data curation, data analysis, and manuscript writing: Luu Van Ninh; Data curation, data analysis: Nguyen Huu Tuan, Le Thi Kim Thoa, Thu-Van Can, Nguyen Ngoc Mong Kha, Bui Xuan Khanh; Manuscript writing and manuscript correction: Thu-Van Can, Doan Quang Tri, Vu Cao Dat; Conceptualisation, manuscript editing and critical evaluation: Doan Quang Tri, Thu-Van Can, Vu Cao Dat.

FUNDING

This study was supported by a research project funded by An Giang Province entitled "*Research on building an early warning system for riverbank erosion in An Giang Province caused by extreme weather phenomena based on artificial intelligence*" (Project Code: 373.2024.02).

CONFLICT OF INTEREST

The authors declare no conflict of interest.

REFERENCES

Abdel Aziz, K. M. (2024). Quantitative monitoring of coastal erosion and changes using remote sensing in a mediterranean delta. Civil Engineering Journal, 10(6), 1842–1862. https://doi.org/10.28991/CEJ-2024-010-06-08.

Al-Zubieri, A. G., Ghandour, I. M., Bantan, R. A. & Basaham, A. S. (2020). Shoreline Evolution Between Al Lith and Ras Mahāsin on the Red Sea Coast, Saudi Arabia Using GIS and DSAS Techniques. Journal of the Indian Society of Remote Sensing, 48, 1455–1470. https://doi.org/10.1007/s12524-020-01169-6.

Alharbi, O. A., Hasan, S. S., Fahil, A. S., Mannaa, A., Buitrago, N. R. & Alqurashi, A. F. (2023). Shoreline change rate detection applying the DSAS technique on low and medium resolution data: Case study along Ash Shu'aybah-Al Mujayrimah coastal Area of the Eastern Red Sea, Saudi Arabia. Regional Studies in Marine Science, 66, 103118. https://doi.org/10.1016/j.rsma.2023.103118.

Bheeroo, R. A., Chandrasekar, N., Kaliraj, S. & Magesh, N. S. (2016). Shoreline change rate and erosion risk assessment along the Trou Aux Biches–Mont Choisy beach on the northwest coast of Mauritius using GIS-DSAS technique. Environmental Earth Sciences, 75, 1–12. https://doi.org/10.1007/s12665-016-5311-4.

Binh, D. V., Wietlisbach, B., Kantoush, S., Loc, H. H., Park, E., Cesare, G. d., Cuong, D. H., Tung, N. X. & Sumi, T. (2020). A novel method for river bank detection from Landsat Satellite Data: A Case Study in the Vietnamese Mekong Delta. Remote Sensing, 12(20), 3298. https://doi.org/10.3390/rs12203298.

Boak, E. H., & Turner, I. L. (2005). Shoreline definition and detection: A review. Journal of Coastal Research, 21(4), 688–703. https://doi.org/10.2112/03-0071.1.

Bordoloi, K., Nikam, B. R., Srivastav, S. K. & Sahariah, D. (2020). Assessment of riverbank erosion and erosion probability using geospatial approach: A case study of the Subansiri River, Assam, India. Applied Geomatics, 12, 265–280. https://doi.org/10.1007/s12518-019-00296-1.

Chalabi, A., Lokman, H. M., Suffian, I. M., Karamali, M., Karthigeyan, V. & Masita, M. (2004). Monitoring Shoreline Change Using IKONOS Image and Aerial Photographs: A Case Study of Kuala Terengganu Area, Malaysia. Proceeding of the 36th International Society for Photogrammetry and Remote Sensing, Part 7, pp. 1–6.

Choi, K. H., Hak-Yang, K., Jung, S. H., Park, S. M. & Lee, S. (2016). Coastal Changes Detected Using Drone-Based Mapping in Hashidong Beach, Gangneung, South Korea. Journal of the Korean Geomorphological Association, 23(4), 101-112. http://dx.doi.org/10.16968/JKGA.23.4.101.

Cuong, V. D., Hung, N. T., Hung, N. V. & Luan, N. T. (2018). Application of remote sensing and gis technologies to study erosion and accretion dynamics in the coastal and estuarine areas of Thua Thien Hue Province. Journal of Water Resources Science and Technology, 1-11. Online available: https://vawr.org.vn/Upload/BaibaoKH/vu-dinh-cuong-48-2018.pdf.

Feng, L., Hu, C., Chen, X., Cai, X., Tian, L. & Gan, W. (2011). Assessment of inundation changes of Poyang Lake using MODIS observations between 2000 and 2010. Remote Sensing of Environment, 121, 80–92. https://doi.org/10.1016/j.rse.2012.01.014.

Hapke, C. J., Brenner, O., Hehre, R. & Reynolds, B. J. (2013). Coastal Change from Hurricane Sandy and the 2012–13 Winter Storm Season: Fire Island, New York. Marine Science Faculty Publications, 2501, pp. 37. https://digitalcommons.usf.edu/msc_facpub/2501/.

Hau, L. M., Hong, N. T. C., Loan, T. T., Duy, D. V., Ty, T. V. (2022). Temporal variation of shoreline position in Vinh Chau District, Soc Trang Province using satellite image analysis. Journal of Hydrometeorology, 733(1), 98–108. https://doi.org/10.36335/VNJHM.2022(733).98-108.

Hladik, C., Alber, M. (2012). Accuracy assessment and correction of a LIDAR-derived salt marsh digital elevation model. Remote Sensing of Environment, 121, 224–235. https://doi.org/10.1016/j.rse.2012.01.018.

Hu, Y., Tian, B., Yuan, L., Li, X., Huang, Y., Shi, R., Jiang, X., Wang, L., Sun, C. (2021). Mapping coastal salt marshes in China using time series of Sentinel-1 SAR. ISPRS Journal of Photogrammetry and Remote Sensing, 173, 122–134. https://doi.org/10.1016/j.isprsjprs.2021.01.003.

Jensen, J. R. (1996). Introductory Digital Image Processing: A Remote Sensing Perspective. 2nd Edition, Prentice Hall, Inc., Upper Saddle River, NJ.

Jia, Y., Liu, Q., He, H., Jin, S., Song, C., Gao, K., Wu, Z. (2026). High accuracy water level estimation using super-resolution Sentinel-1 data. International Journal of Applied Earth Observation and Geoinformation, 146, 105156. https://doi.org/10.1016/j.jag.2026.105156.

Karnata, S., Kumari, N. (2025). Application of Geospatial Technologies and AI to Detect and Analyze the Shoreline Change of Visakhapatnam, a Coastal District. In: Sarif, M.O., Sharifi, A. (eds) Advanced Geospatial Intelligence and AI for Environmental Resilience and Sustainable Development. Advances in Geographic Information

Science. Springer, Cham, pp. 265–290. https://doi.org/10.1007/978-3-032-03714-5_12.

Khoi, D. N., Dang, T. D., Pham, L. T. H., Loi, P. T., Thuy, N. T. D., Phung, N. K., Bay, N. T. (2020). Morphological change assessment from intertidal to river-dominated zones using multiple-satellite imagery: a case study of the Vietnamese Mekong Delta. Regional Studies in Marine Science, 34, 101087. https://doi.org/10.1016/j.rsma.2020.101087.

Kish, S. A. & Donoghue, J. F. (2013). Coastal response to storms and sea-level rise: Santa Rosa Island, Northwest Florida, U.S.A. Journal of Coastal Research, 63, 131–140. https://doi.org/10.2112/SI63-012.1.

Li, X., Liu, J. P., Saito, Y. & Nguyen, V. L. (2017). Recent evolution of the Mekong Delta and the impacts of dams. Earth-Science Reviews, 175, 1–17. https://doi.org/10.1016/j.earscirev.2017.10.008.

Liu, H. (2009). Shoreline Mapping and Coastal Change Studies Using Remote Sensing Imagery and LIDAR Data. In: Yang, X. (eds) Remote Sensing and Geospatial Technologies for Coastal Ecosystem Assessment and Management. Lecture Notes in Geoinformation and Cartography. Springer, Berlin, Heidelberg, pp. 297–232. https://doi.org/10.1007/978-3-540-88183-4_13.

Long, N. D. H. & Khoi, D. N. (2020). Using landsat satellite images for assessing riverbank changes in the Mekong and Bassac rivers in the An Giang province. Science & Technology Development Journal – Engineering and Technology, 2(SI2), SI53-SI62. https://doi.org/10.32508/stdjet.v2iSI2.444.

Long, V. H., Giang, N. V., Hoanh, T. P., Hoa, P. V. (2019). Applying google earth engine in river bank erosion monitoring – A case study in lower Mekong river. Journal of Sciences Natural Sciences and Technology, 16(6), 38-49. Online available: https://vjol.info.vn/index.php/sphcm/article/view/40986/32913.

Marfai, M. A., Almohammad, H., Dey, S., Susanto, B. & King, L. (2008). Coastal Dynamic and Shoreline Mapping: Multi-Sources Spatial Data Analysis in Semarang Indonesia. Environmental Monitoring and Assessment, 142(1–3), 297–308, https://doi.org/10.1007/s10661-007-9929-2.

McFeeters, S. K. (2007). The use of the Normalized Difference Water Index (NDWI) in the delineation of open water features. International Journal of Remote Sensing, 17(7), 1425–1432. https://doi.org/10.1080/01431169608948714.

Miah, M.D., Chowdhury, N.A. & Ali, Y. (2025). Monitoring multi-decadal riverbank dynamics of the Padma river in Bangladesh using geospatial analysis and DSAS model. Discover Geoscience, 3, 238. https://doi.org/10.1007/s44288-025-00353-w.

Mishra, M., Kar, D., Santos, C.A.G., da Silva, R. M. & Das, P. P. (2022). Assessment of impacts to the sequence of the tropical cyclone Nisarga and monsoon events in

shoreline changes and vegetation damage in the coastal zone of Maharashtra, India. Marine Pollution Bulletin, 174, 113262. https://doi.org/10.1016/j.marpolbul.2021.113262.

Moore, L. J. (2000). Shoreline mapping techniques. Journal of Coastal Research, 16(1), 111–124. https://www.jstor.org/stable/4300016.

Morton, R., Miller, T. & Moore, L. (2005). Historical shoreline changes along the US Gulf of Mexico: A summary of recent shoreline comparisons and analyses: Journal of Coastal Research, 21(4), 704–709. https://doi.org/10.2112/04-0230.1.

Novais, J., Vieira, A., Bento-Gonçalves, A., Silva, S., Folharini, S., & Marques, T. (2023). The Use of UAVs for Morphological Coastal Change Monitoring—A Bibliometric Analysis. Drones, 7(10), 629. https://doi.org/10.3390/drones7100629.

Phuong, P. V. T., Hanh, P. T. H., Long, B. T. (2023). Application of remote sensing, GIS to assess the rate and range of coastal erosion in the Mekong River Delta, from Tien Giang to Soc Trang Province. Journal of Hydro-Meteorology, 754, 9–25. https://doi.org/10.36335/VNJHM.2023(754).9-25.

Puttinaovarat, S., Saeliw, A., Pruitikanee, S., Kongcharoen, J., Chai-Arayalert, S., Khaimook, K., Horkaew, P. (2021). River classification and change detection from landsat images by using a river classification toolbox. IAES International Journal of Artificial Intelligence (IJ-AI), 10(4), 948–959. https://doi.org/10.11591/ijai.v10.i4.pp948-959.

Quynh, H. N. N., Khoi, D. N., Hoai, H. C., Bay, N. T. (2018). Application of remote sensing and gis for riverbank assessment in the Bassac and Mekong rivers. Journal of Hydro-Meteorology, 691, 12–22. Online available: http://tapchikttv.vn/article/148.

Quynh, C. K. N., Hanh, P. T. H., Long, B. T. (2022). Assessment of the shoreline evolution and coastal erosion trends along Cua Dai beach, Hoi An City, Quang Nam. Journal of Hydro-Meteorology, 736(1), 41–53. Online available: http://tapchikttv.vn/article/1974.

Shin, B. & Kim, K. (2015). Estimation of Shoreline Change Using High Resolution Images, 8 th International Conference on Asian and Pacific Coasts. Procedia Engineering, 116, 994–1001. https://doi.org/10.1016/j.proeng.2015.08.391.

Son, P. Q. et al. (2015). Final report of the project: “Research on the application of VNREDSat-1 and equivalent satellite imagery for the investigation, forecasting, and assessment of geological hazards affecting hydropower reservoirs and transportation infrastructure in the Northwestern provinces of Vietnam”. Project code: VT/UD-03/13-15. Institute of Geological Sciences, Vietnam Academy of Science and Technology.

Sujivakand, J., Samarasekara, R. S. M., Siriwardana, H. P. A. M., Anthony, D. R., Siriwardana, H. (2024). Unmanned aerial vehicles (UAVs) for coastal protection assessment: A study of detached breakwater and groins at Marawila Beach, Sri Lanka. Regional Studies in Marine Science, 69, 103282. https://doi.org/10.1016/j.rsma.2023.103282.

Tamassoki, E., Amiri, H., Soleymani, Z. (2014). Monitoring of Shoreline Changes Using Remote Sensing (Case Study: Coastal City of Bandar Abbas). Proceeding of the 7th IGRSM International Remote Sensing & GIS Conference and Exhibition, IOP Conf. Series: Earth and Enviromental Science, 20, 012023. https://doi.org/10.1088/1755-1315/20/1/012023.

Tan, B., Cooper, H., Bartley, M. L., Johnson, C., Fagherazzi, S., Fichot, C. (2026). Monitoring Coastal Shoreline Change using PlanetScope Imagery. Estuarine, Coastal and Shelf Science, 109783. https://doi.org/10.1016/j.ecss.2026.109783.

Tinh, T. V. & Phong, D. H. (2017). Applying remote sensing and gis for study change in coastalareas of Ca Mau Cape. Journal of Hydro-Meteorology, 684, 35-40. Online available: http://tapchikttv.vn/article/244.

Tha, T., Piman, T., Bhatpuria, D. & Ruangrassamee, P. (2022). Assessment of riverbank erosion hotspots along the Mekong River in Cambodia using remote sensing and hazard exposure mapping. Water, 14(13), 1981. https://doi.org/10.3390/w14131981.

Thao, P. T. P., Duan, H. D. & To, D. V. (2011). Application of Remote Sensing and GIS for Calculating the Coastline Changes in Phan Thiet. Vietnam Journal of Marine Science and Technology, 11(3), 1–13. https://doi.org/10.15625/1859-3097/11/3/375.

Thakur, S., Dey, D., Dá, P., Ghosh, P. B. & De, T. K. (2017). Shoreline change detection using Remote Sensing in the Bakkhali Coastal Region, West Bengal, India. Indian Journal of Geosciences, 71(4), 611–626.

Thi, T. N. K. & Thu, P. T. M. (2019). Application of remote sensing and gis to assess of the change of da rang river mouth area, at Phu Yen province. Proceeding of the GIS conference at Daklak, Vietnam.

Thieler, E. R., Himmelstoss, E. A., Zichichi, J. L., & Ergul, A. (2009). The Digital Shoreline Analysis System (DSAS) version 4.0 - An ArcGIS extension for calculating shoreline change. U.S. Geological Survey Open-File Report 2008-1278. https://doi.org/10.3133/ofr20081278.

Thuy, V. T. T. (2012). Application of Remote Sensing and GIS Technologies for Studying Coastal Erosion and Accretion Hazards in the Hai Phong Coastal Zone. Master's Thesis. University of Science, Vietnam National University, Hanoi. Code: 604455, pp. 70.

Thuy, N. T. D., Khoi, D. N., Nhan, D. T., Nga, T. N. Q., Bay, N. T. & Phung, N. K. (2019). Modelling accretion and erosion processes in the Bassac and Mekong Rivers of the Vietnamese Mekong Delta, in: Viet, N.T., Xiping, D., Tung, T.T. (Eds.). Proceeding of the 10th International Conference on Asian and Pacific Coasts, Hanoi, Vietnam, Springer, Hanoi, pp. 1431–1437.

Tri, D. Q., Nhat, N. V., Cuong, V. D. (2023). Application of deep learning and remote sensing to assess the riverbank change: A case study at Nhat Le river mouth, Viet Nam. Proceeding of the Earth and Environmental Sciences, Mining for Digital Transformation, Green Development, and Response to Global Change (GREEN EME 2023), December 29, 2023, pp. 215-226.

Trung, N. V. & Khanh, N. V. (2016). Monitoring coastline changes using landsat multi-temporal data in the Cua Dai estuary, Thu Bon river, Quang Nam. Journal of Mining and Earth Sciences, 57, 81–89. Online available: https://jmes.humg.edu.vn/images/paper/So12-nguyenvantrung-81_89.pdf.

Tung, T. T., Hung, T. D. (2023). A study on using Sentinel 2 imagery to analyse shoreline change and nearshore topography evolution in the Nhat Le estuary, Quang Binh province. Journal of Hydro-Meteorology, 746, 1–11. https://doi.org/10.36335/VNJHM.2023(746).1-11.

USGS (2021). Digital Shoreline Analysis System (DSAS) v5.0. U.S. Geological Survey.

Xu, H. (2007). Modification of normalized difference water index (NDWI) to enhance open water features in remotely sensed imagery. International Journal of Remote Sensing, 27(14), 3025–3033. https://doi.org/10.1080/01431160600589179.

Authors' Contribution

All authors contributed equally to the development of this article.

Data availability

All datasets relevant to this study's findings are fully available within the article.

How to cite this article (APA)

Ninh, L. V., Tuan, N. H., Thoa, L. T. K., Tri, D. Q., Dat, V. C., Kha, N. N. M., … Can, T.-V. (2026). APPLYING REMOTE SENSING IMAGE INTERPRETATION TO ANALYZE RIVERBANK CHANGES: A CASE STUDY IN THE MEKONG DELTA. *Veredas Do Direito*, *23*(6), e235894. https://doi.org/10.18623/rvd.v23.5894